ORIGINAL ARTICLE

The Organization of the Human Corpus Callosum Estimated by Intrinsic Functional Connectivity with White-Matter Functional Networks

Pan Wang[1], Chun Meng[1], Rui Yuan[2], Jianlin Wang[1], Hang Yang[1], Tao Zhang[1], Laszlo Zaborszky[3], Tara L. Alvarez[4], Wei Liao[1], Cheng Luo[1], Huafu Chen[1] and Bharat B. Biswal[1,4]

[1]The Clinical Hospital of Chengdu Brain Science Institute, MOE Key Laboratory for Neuroinformation, Center for Information in Medicine, School of Life Science and Technology, University of Electronic Science and Technology of China, Chengdu 611731, China, [2]Department of Psychiatry, Stanford University, Palo Alto, CA 94305, USA, [3]Center for Molecular and Behavioral Neuroscience, Rutgers University, Newark, NJ 07102, USA and [4]Department of Biomedical Engineering, New Jersey Institute of Technology, Newark, NJ 07102, USA

Address correspondence to Bharat B. Biswal, Department of Biomedical Engineering, New Jersey Institute of Technology, 607 Fenster Hall, University Height, Newark, NJ 07102, USA. Email: bbiswal@yahoo.com; Chun Meng, The Clinical Hospital of Chengdu Brain Science Institute, MOE Key Laboratory for Neuroinformation, Center for Information in Medicine, School of Life Science and Technology, University of Electronic Science and Technology of China, No. 2006, Xiyuan Avenue, Chengdu 611731, China. Email: chunmeng@uestc.edu.cn.

Abstract

The corpus callosum is the commissural bridge of white-matter bundles important for the human brain functions. Previous studies have analyzed the structural links between cortical gray-matter networks and subregions of corpus callosum. While meaningful white-matter functional networks (WM-FNs) were recently reported, how these networks functionally link with distinct subregions of corpus callosum remained unknown. The current study used resting-state functional magnetic resonance imaging of the Human Connectome Project test–retest data to identify 10 cerebral WM-FNs in 119 healthy subjects and then parcellated the corpus callosum into distinct subregions based on the functional connectivity between each callosal voxel and above networks. Our results demonstrated the reproducible identification of WM-FNs and their links with known gray-matter functional networks across two runs. Furthermore, we identified reliably parcellated subregions of the corpus callosum, which might be involved in primary and higher order functional systems by functionally connecting with WM-FNs. The current study extended our knowledge about the white-matter functional signals to the intrinsic functional organization of human corpus callosum, which could help researchers understand the neural substrates underlying normal interhemispheric functional connectivity as well as dysfunctions in various mental disorders.

Key words: corpus callosum, fMRI, HCP test–retest data, intrinsic functional organization, white-matter functional networks

Introduction

Functional magnetic resonance imaging (fMRI) detects hemodynamic changes associated with neural activity based on the blood-oxygenation-level-dependent (BOLD) signals (Ogawa et al. 1990). Using the BOLD signals, we can assess temporally synchronized brain activity across local brain regions (Biswal et al. 1995; Lowe et al. 1998). However, most of these studies in fMRI have primarily focused on the gray-matter BOLD signals. The

signals from the white-matter have usually been considered to be noise dominated and rarely reported in the literatures. Recent studies have demonstrated the presence of small yet reliable changes in specific white-matter regions responding to tasks (Ji et al. 2017; Marussich et al. 2017). A few studies have also demonstrated neural-driven white-matter signal fluctuations during rest (Peer et al. 2017; Ding et al. 2018; Jiang et al. 2019).

Given that white matter densely connects different regions of the gray matter and accounts for nearly half of the human brain (Teo et al. 1997; Zhang and Sejnowski 2000; Arai and Lo 2009; Harris and Attwell 2012), a few researchers have explored the relationship between white-matter networks and gray-matter networks based on resting-state functional connectivity in normal and clinical populations. Ding and colleagues have found that BOLD signals in certain white-matter tracts are functionally correlated with specific gray-matter regions during different tasks (Ding et al. 2018). Moreover, Peer and colleagues demonstrated the presence of distinct symmetric white-matter functional networks (WM-FNs) in resting-state fMRI signals, which were closely related to both gray-matter functional networks (GM-FNs) and the underlying structural white-matter tracts (Peer et al. 2017). They suggested that the interaction between the WM- and GM-FNs provide clues as to how these spatially networks were connected. On the other hand, the symmetric WM-FNs corresponding to the gray-matter perception-motor system were altered in patients with schizophrenia, which demonstrates that connections between the WM- and GM-FNs are necessary to maintain the normal functionality of the brain (Jiang et al. 2019).

As the largest white-matter fiber bundle, the corpus callosum connects the two hemispheres of human brain and contains more than 250 million axons (Nolte 2002). Thus, the corpus callosum plays a crucial role in transmitting sensory, motor, and cognitive information between homotopic regions of the two cerebral hemispheres (Gazzaniga 2000). It has been demonstrated that a larger callosal area has a performance advantage in cognitive tasks (Berlucchi 1983; Yazgan et al. 1995). Because the primary function of corpus callosum is to act as the primary cortical projection system (Rosas et al. 2010), any focal or diffuse abnormalities of the bilaterally connected cortical regions may result in the secondary effects on homotopically distributed fibers in the callosum. For example, patients with schizophrenia have been reported to have a statistically significant reduction in cortical area within the corpus callosum compared to healthy controls (Woodruff et al. 1995). Patients with attention-deficit hyperactivity disorder have been shown to have a smaller area in the rostrum and rostral body of corpus callosum compared to healthy controls (Giedd et al. 1994; Baumgardner et al. 1996). Patients with Alzheimer's disease are reported to have atrophy of corpus callosum (Vermersch et al. 1996). A range of neurodevelopmental disorders and dysplasias has been reported to lead to corpus callosum agenesis (Sebire et al. 1995). Moreover, the morphologic anomalies of corpus callosum have also been reported for a wide variety of childhood neuropsychiatric illness and sexual dimorphism (Giedd et al. 1999).

Several studies on the structure of the corpus callosum have divided the corpus callosum into different subregions that connects bilateral corresponding cortical areas in the brain (Aboitiz et al. 1992; Huang et al. 2005; Chao et al. 2009). For instance, by using light microscopic examination in 10 regions of the corpus callosum, Aboitiz and colleagues found the regional differentiation of fiber types in the corpus callosum (Aboitiz et al. 1992). Huang and colleagues divided the corpus callosum

into six major subdivisions based on trajectories to different cortical areas by using DTI tractography (Huang et al. 2005). In addition, the corpus callosum was parcellated into different subregions based on its cortical trajectories to specific cytoarchitectural regions using HARDI-based tractography and tract-based transformation (Chao et al. 2009). It has been shown that distinct regions of the corpus callosum were activated during different tasks, such as motor, tactile, visual, auditory, gustatory, and memory task (Mazerolle et al. 2008; Yarkoni et al. 2009; Fabri et al. 2011). Moreover, these activation foci in the corpus callosum were distributed according the anterior (taste stimuli), middle (motor task), middle and posterior (tactile stimuli) and splenium (visual stimuli) (Fabri et al. 2011). These cumulative findings support that the subregions of the corpus callosum are associated with the distinct functions of the human brain. Although the corpus callosum has been structurally parcellated into different subregions, the underlying BOLD fMRI signals in the corpus callosum and how functional information is transferred within the corpus callosum and other brain regions have not been investigated.

Therefore, we hypothesize that the corpus callosum may be differentially connected with WM-FNs. To address this hypothesis, we evaluated the WM-FNs by performing a clustering analysis to the voxel-based white-matter functional connectivity matrix, and studied the relationships between WM- and GM-FNs. Subsequently, we used partial correlation analysis to explore the connectivity between the WM-FNs and each voxel in the corpus callosum. Using a winner-take-all algorithm, each callosal voxel was assigned to a single WM-FN with the most similar profile of connectivity. In this way, we identified the subregions of corpus callosum related to specific WM-FNs. In the end, to assess the reproducibility of our findings, we validated the WM-FNs and divided the corpus callosum in different datasets.

Materials and Methods

Data Acquisition

This study employed the test–retest dataset from the Human Connectome Project (HCP) dataset (https://db.humanconnectome.org). The datasets of 129 healthy subjects were used in this study, including both resting-state fMRI and T1-weighted anatomical scans from two different days, which had four runs (rfMRI_rest1_LR, rfMRI_rest1_RL, rfMRI_rest2_LR, and rfMRI_rest2_RL). Rest1 and Rest2 were acquired on different days. We chose the two runs of data for the current analysis including the rfMRI_rest1_LR and rfMRI_rest2_LR. The HCP scanning protocol was approved by the local Institutional Review Board at Washington University in St. Louis. All subjects signed an informed consent. Imaging data were collected on a customized Siemens 3-T Connectome-Skyra scanner. Because details about the imaging parameters have been described elsewhere in detail (Van Essen et al. 2013), it is briefly described here. The imaging parameters used to collect the rfMRI data were as follows: TR = 0.72 s; TE = 33.1 ms; flip angle = 52°; field of view = 208 × 180 mm^2; slice number = 72; functional spatial resolution = 2 mm isotropic voxel; multiband factor = 8; echo spacing = 0.58 ms; bandwidth = 2290 Hz/px; volumes = 1200.

Data Preprocessing

Functional images were preprocessed by using the Data Processing Assistant for Resting-State fMRI (http://rfmri.org/

DPARSF) and SPM12 software (http://www.fil.ion.ucl.ac.uk/spm/software/spm12). The data preprocessing included following steps. First, we discarded the first 10 volumes, correction for head-motion-related signal changes. Subjects with maximum displacements greater than 3 mm or 3° were excluded from further analyses, resulting in a cohort of 119 subjects out of the original 129 subjects. Each individual's T1-weighted MPRAGE image was co-registered to the mean functional image using a 6 degree-of-freedom linear transformation without re-sampling. Each structural image was segmented into gray matter (GM), white matter (WM), and cerebrospinal fluid (CSF), to obtain the transformation from native to standard MNI space. Linear trends were removed. Signal from CSF and 24 rigid body motion parameters (6 head motion parameters, 6 head motion parameters one time point before, and the 12 corresponding squared items) were regressed from the data. To reduce the impact of head motion, scrubbing using motion "spikes" was performed as separate regressors identified by framewise displacement (FD) greater than 1 mm. The head motion scrubbing regressors were used in this study as it has been shown to be effective in reducing the effect of head motion at the spike on the signal without changing the correlation values (Power et al. 2012; Satterthwaite et al. 2013). To retain as much of the signal of interest as possible, the white-matter and global mean signals were not regressed from the dataset. Temporal filtering was done in the low-frequency range of 0.01–0.15 Hz in line with prior white-matter functional connectivity studies to reduce non-neuronal contribution to BOLD fluctuations (Peer et al. 2017; Jiang et al. 2019). To avoid mixing white-matter and gray-matter signals, the functional images were minimally spatially smoothed separately (4-mm full-width half-maximum [FWHM], isotropic) within the white-matter and gray-matter templates for each subject. The white-matter and gray-matter voxels were identified by using the segmentation results from each subject (using a threshold of 0.5 using SPM12's tissue segmentation) (Peer et al. 2017; Jiang et al. 2019). Finally, we merged the white-matter and gray-matter images into full functional images using the smoothed data. Following smoothing, the functional images were transformed from individual native space into MNI space with a voxel size of $3 \times 3 \times 3$ mm^3.

The Creation of Group White-matter Mask

To obtain group white-matter mask for clustering across the group, segmentation was used for each subject's dataset to minimize the influence from other signal sources, particularly the gray matter. Specifically, for each subject, we identified each voxel in the whole brain as belonging to one of the following three classes: white matter, gray matter, or CSF based on the maximum probability from the three segmentation images. This step generated a binarized white-matter mask for each subject. Then, these masks were averaged across all subjects. The voxels with a ratio of subjects greater than 60% were considered as white-matter voxels in the T1 images. The voxels of resulting mask were then selected and identified as the white-matter mask in greater than 80% of subjects in the functional data. Finally, the Harvard-Oxford Atlas (Desikan et al. 2006) was utilized to correctly classify the deep brain structures (Babalola et al. 2010; Lorio et al. 2016).

The Corpus Callosum Mask

We obtained the corpus callosum mask from the JHU ICBM-DTI-81 WM atlas (Mori et al. 2008). To minimize the effect of the gray
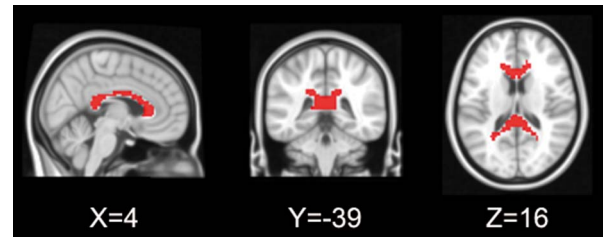

Figure 1. Corpus callosum mask obtained from the JHU ICBM-DTI-81WM atlas. The group level white-matter mask is used to limit the size of corpus callosum.

matter, we used the group white-matter mask to limit the size of corpus callosum (Fig. 1).

Clustering WM-FNs in the Group White-Matter Mask

Since our study aimed to explore the correlation between the WM-FNs and corpus callosum, we excluded these voxels of corpus callosum in the group white-matter mask using the corpus callosum mask. To reduce the calculative complexity of clustering, we used an interchanging grid to subsample the white-matter mask (including 16 839 voxels). Every second voxel along the image rows and columns were taken and shifted by 1 between slices to reduce missing columns of data. Then, we could obtain a subsampled mask including 4192 voxels. Pearson's correlation coefficient was computed between each of the white-matter voxel time series and all of the subsampled mask voxels, resulting in a white-matter correlation pattern for each voxel (16 839 × 4192) (Yeo et al. 2011; Craddock et al. 2012). To obtain a group-level correlation matrix, the correlation matrices for each subject was calculated and then averaged across all 119 subjects. K-means clustering (distance metric correlation, 10 replications) was performed on the group-level voxelwise correlation matrix to obtain the WM-FNs (Blumensath et al. 2013; Yeo et al. 2014). The numbers of clusters were chosen from 2 to 22, and the stability of each cluster was analyzed to get the optimal number of WM-FNs (Yeo et al. 2011). Specifically, the group-level correlation matrix was randomly divided into fourfolds. For each number of clusters, we computed the clustering process on each fold separately and analyzed the similarity. To analyze the similarity of clustering in different folds, we calculated an adjacency matrix for each fold and compared them using Dice coefficient. The average Dice coefficient computed by comparing each other in all four adjacency matrices was computed to detect the stability for each number clustering (Yeo et al. 2011). A number of stable clusters were found at 4, 7, 9, and 12 clusters, and then we chose the most detailed level (12 WM-FNs) (Fig. S1–1). Finally, we kept 10 WM-FNs for further analysis and excluded two white-matter cerebellum networks, since we focused on the cortex within this study. To test the reproducibility between the two runs, we obtained the WM-FNs using the clustering method from run 1 and reanalyzed the correlation between the WM-FNs and the corpus callosum for each of the two runs. We also obtained 12 WM-FNs using the clustering method in the run 2 and analyzed the spatial overlap for different WM-FNs between two runs (Fig. S2–1).

Functional Connectivity of WM-FNs

To study the correlation between WM- and GM-FNs, Pearson's correlation coefficient was calculated between each averaged

WM- and GM-FNs time series for each subject. The GM-FNs atlas employed in this study was the same with that used in previous studies (Peer et al. 2017; Jiang et al. 2019). In addition, we also obtained 7 GM-FNs using present data and analyzed the correlation between WM-FNs and new GM-FNs (Figs S4–1 and S4–2). To analyze the correlation between different WM-FNs, we calculated the Pearson's correlation coefficient between averaged WM-FNs time series.

The Functional Parcellation of Corpus Callosum

Functional connectivity between the 10 WM-FNs, and each voxel in the corpus callosum was used to identify the different sub-regions of the corpus callosum. Specifically, partial correlation analysis was calculated between the averaged time course of each WM-FN and every voxel time course in the corpus callosum mask, while controlling for the effect of all other nine WM-FNs. All the correlation coefficients were then Fisher-transformed to Z-scores. A one-sample t-test was calculated across all participants, resulting in a statistical t-map of connectivity pattern for each WM-FN as region of interest (ROI). A "winner-take-all" algorithm was adopted such that each callosal voxel was assigned to a single WM-FN with the most similar profile of connectivity. To have a more comprehensive understanding of the relation between the corpus callosum and those 10 WM-FNs, we performed a statistical correction to the one-sample t-test map of each WM-FN as ROI ($P < 0.05$, Family Wise Error (FWE) corrected). To explain the reproducibility of our results, these analyses were performed on run 1 and run 2 data separately.

Measures of Reproducibility

To estimate the similarity of callosal subregions and WM-FNs between two runs, we introduced the Dice coefficient. The Dice coefficient was calculated according to the standard formula:

$$\text{Dice}(V_1, V_2) = \frac{2 \mid V_1 \cap V_2 \mid}{\mid V_1 \mid + \mid V_2 \mid}$$

where V_1 is the dataset from run 1 and V_2 is the dataset from run 2. The Dice coefficient was 2categorized approximately as follows: low (0–0.19), low moderate (0.2–0.39), moderate (0.4–0.59), moderate high (0.6–0.79), or high (0.8–1) in line with prior study (Wilson et al. 2017).

To analyze the reproducibility of the functional connectivity between WM-FNs, we calculated the Pearson's correlation coefficient between averaged functional connectivity matrices from two runs. Similarly, the reproducibility of the functional connectivity between the WM- and GM-FNs was also analyzed. Finally, to analyze whether current method was suitable for studies with small number of subjects, we repeated the clustering for WM-FNs and parcellation procedures in different sample sizes (1, 5, 10, 20, 30, 40, 50, 60, 70, 80, 90, 100, and 110) (Figs S5–1 and S5–2).

Results

Identification of WM-FNs

The WM-FNs were identified by using K-means clustering on the averaged functional connectivity matrix. The clustering and the Dice coefficient results showed that the largest number of WM-FNs was 12, which was selected for identifying final clustering results (Fig. S1–1). The final WM-FNs involved two cerebellar

networks and 10 cerebral networks (Fig. 2). Except for the left prefrontal network, the resulting WM-FNs showed an interlaced and a relatively symmetric pattern. The WM-FNs in run 2 similar to the WM-FNs from run 1 were reproduced on the resting-state fMRI dataset of run 2 (Fig. S2–1).

Reproducibility of Functional Connectivity of WM-FNs

Our study found strong correlations between different WM-FNs, including the deep, occipital, orbitofrontal, anterior corona radiata, sensorimotor middle, posterior corona radiata, and sensorimotor superficial WM-FNs (Fig. 3A,C). Pearson's correlation coefficient was computed on the two averaged functional connectivity matrices between two runs to show the reproducibility of functional connectivity. The functional connectivity between WM-FNs was reproducible in two runs ($r > 0.99$). In addition, we also estimated the relationship between the WM- and GM-FNs. The tempofrontal, occipital, and sensorimotor superficial WM-FNs exhibited high functional connectivity ($r > 0.9$) with the gray-matter default mode network (DMN), visual network, and sensorimotor network, respectively. Moreover, the functional connectivity between WM- and GM-FNs was reproducibility between two runs ($r > 0.99$).

Functional Connectivity between the WM-FNs and Corpus Callosum

Since WM-FNs were reproducibly identified in the bilateral hemispheres, we further tested how WM-FNs were related to interhemispheric connections, by examining functional connectivity between WM-FNs and each voxel of corpus callosum. Based on the geometrical landmark defined by Witelson and colleagues, the corpus callosum can be divided into seven subregions based on the length of corpus callosum including the rostrum, genu, rostral body, anterior midbody, posterior midbody, isthmus, and splenium of the corpus callosum (Witelson 1989). We found that the WM-FNs significantly connected to the different regions of corpus callosum (after thresholding by winner-take-all) (Fig. 4, Table 1). Specifically, the left prefrontal WM-FN correlated with the anterior midbody of corpus callosum. The callosal subregions corresponding to tempofrontal WM-FN concentrated mainly on the splenium and genu. The subregions relating with deep WM-FN had distributions in the anterior midbody, isthmus, posterior midbody, and rostral body of corpus callosum. Occipital WM-FN was only connected with the splenium of corpus callosum. The orbitofrontal WM-FN was mainly associated with the rostral and genu of corpus callosum. The regions corresponding to anterior corona radiata WM-FN distributed in seven areas of corpus callosum. The voxel of corpus callosum associated with the sensorimotor middle WM-FN mainly distributed in the anterior midbody, isthmus, and posterior midbody of corpus callosum. Finally, the posterior corona radiata WM-FN was related with the isthmus and splenium of corpus callosum. No voxels in the corpus callosum corresponded to sensorimotor superficial WM-FN. The callosal regions corresponding to inferior corticospinal WM-FN exhibited differences between two runs. The inferior corticospinal WM-FN was associated with isthmus and splenium of corpus callosum in the run 1 data. However, there were no voxels corresponding to the inferior corticospinal WM-FN in the run 2 data. More details about the correlation between the corpus callosum and WM-FNs were shown in the Table 1.
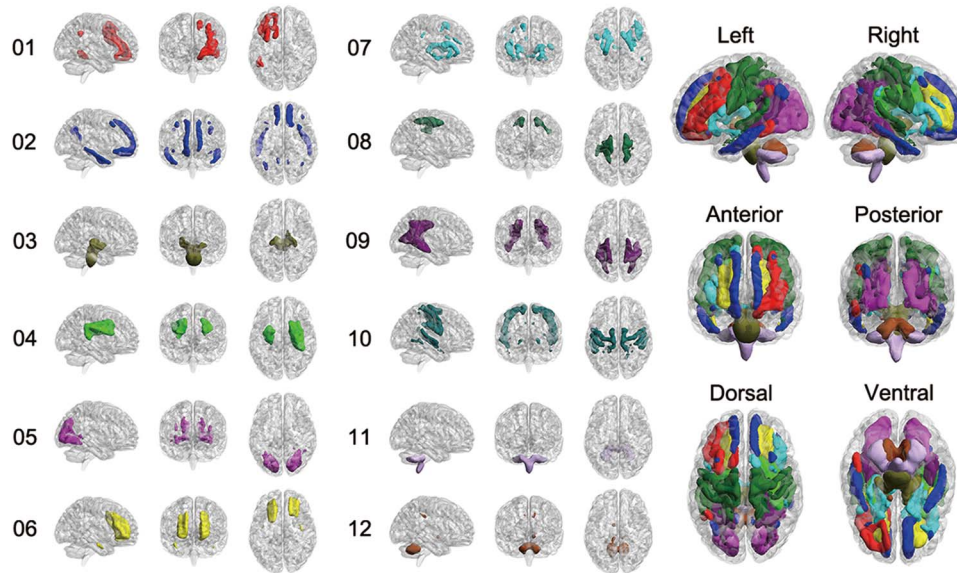
Figure 2. WM-FNs identified using K-means clustering method. 01. Left prefrontal WM-FN; 02. Tempofrontal WM-FN; 03. Inferior corticospinal WM-FN; 04. Deep WM-FN; 05. Occipital WM-FN; 06. Orbitofrontal WM-FN; 07. Anterior corona radiata WM-FN; 08. Sensorimotor middle WM-FN; 09. Posterior corona radiata WM-FN; 10. Sensorimotor superficial WM-FN; 11. Cerebellar inferior WM-FN; 12. Cerebellar superior WM-FN.

Reproducibility of Functional Connectivity between WM-FNs and Corpus Callosum

To detect the reproducibility of the correlation between the WM-FNs and corpus callosum, the Dice coefficient was computed on the result regions of corpus callosum corresponding to each WM-FN between two runs. The spatial overlap for callosal subregions corresponding to each WM-FN showed different levels that were classified as moderate, moderate-high, and high (Fig. 5). Specifically, the subregions of corpus callosum corresponding to these four WM-FNs had a high Dice coefficient between two runs (The Dice coefficients for callosal subregions corresponding to the deep, occipital, orbitofrontal, and posterior corona radiata WM-FNs were found to be 0.84, 0.80, 0.92, and 0.90, respectively.) The subregions of corpus callosum associated with these three WM-FNs revealed a moderate-high Dice coefficient between two runs (The Dice coefficients for callosal subregions corresponding to the tempofrontal, anterior corona radiata, and sensorimotor middle WM-FNs were found to be 0.76, 0.64, and 0.61, respectively.) Finally, we found that the subregions of corpus callosum linking the left prefrontal WM-FN had only a moderate level overlap between two runs (The Dice coefficient for callosal subregion corresponding to the left prefrontal WM-FN was 0.40.) We did not show the results of Dice coefficient corresponding to the callosal subregions related to the inferior corticospinal and sensorimotor superficial WM-FNs in the Figure 5, because there were no relevant voxels between these two WM-FNs and corpus callosum calculated using run 2 data.

Further Explorations of the Correlation between the WM-FNs and Corpus Callosum

The one-sample t-test maps and resulting callosal subregions ($P < 0.05$, FWE corrected), corresponding to the inferior corti-cospinal, sensorimotor superficial, and inferior corticospinal WM-FNs, were shown in Figure 6. The remaining maps of callosal subregions after correction corresponding to other seven WM-FNs were shown in the Figure S3–1. The Dice coefficient was calculated to the maps of callosal subregions corrected by FWE ($P < 0.05$) corresponding to each WM-FN between two runs. The subregions of corpus callosum associated with these two WM-FNs (the left prefrontal and sensorimotor superficial WM-FNs) revealed a moderate–high Dice coefficient between two runs. The subregions of corpus callosum linking the inferior corticospinal WM-FN had a low-moderate level overlap between two runs.

Discussion

This study used temporal correlation between voxelwise time series BOLD signals from the white matter and corpus callosum to demonstrate novel concordance between them. Our findings demonstrated that corpus callosum had a functional segmentation and unique spatial distribution patterns with WM-FNs. Furthermore, this study confirmed a close relationship between the WM- and GM-FNs in line with recent studies. Different subregions of the corpus callosum might connect the specific WM-FNs to further associate with the cerebral cortex, and use this way to transmit sensory, motor, and cognitive information between homotopic regions of the two cerebral hemispheres. In the end, the correlation between the WM-FNs and corpus callosum was found reproducible by using two runs of HCP data with same subjects.

Increasing studies have shown meaningful functional activity in the white-matter regions, like stimulus-induced activations in the white matter (Gawryluk et al. 2014; Ji et al. 2017; Marussich et al. 2017; Wu et al. 2017; Courtemanche et al. 2018). For instance, Huang and colleague have demonstrated that white-matter voxels were activated mostly along the fiber pathways relevant to visual activity (Huang et al. 2018). Here, we identified 10 WM-FNs, which were consistent with previous studies (Fig. 2) (Peer et al. 2017). We found that WM-FNs showed a close relationship with GM-FNs (Fig. 3B,D). Specifically, the tempofrontal, occipital, and sensorimotor superficial
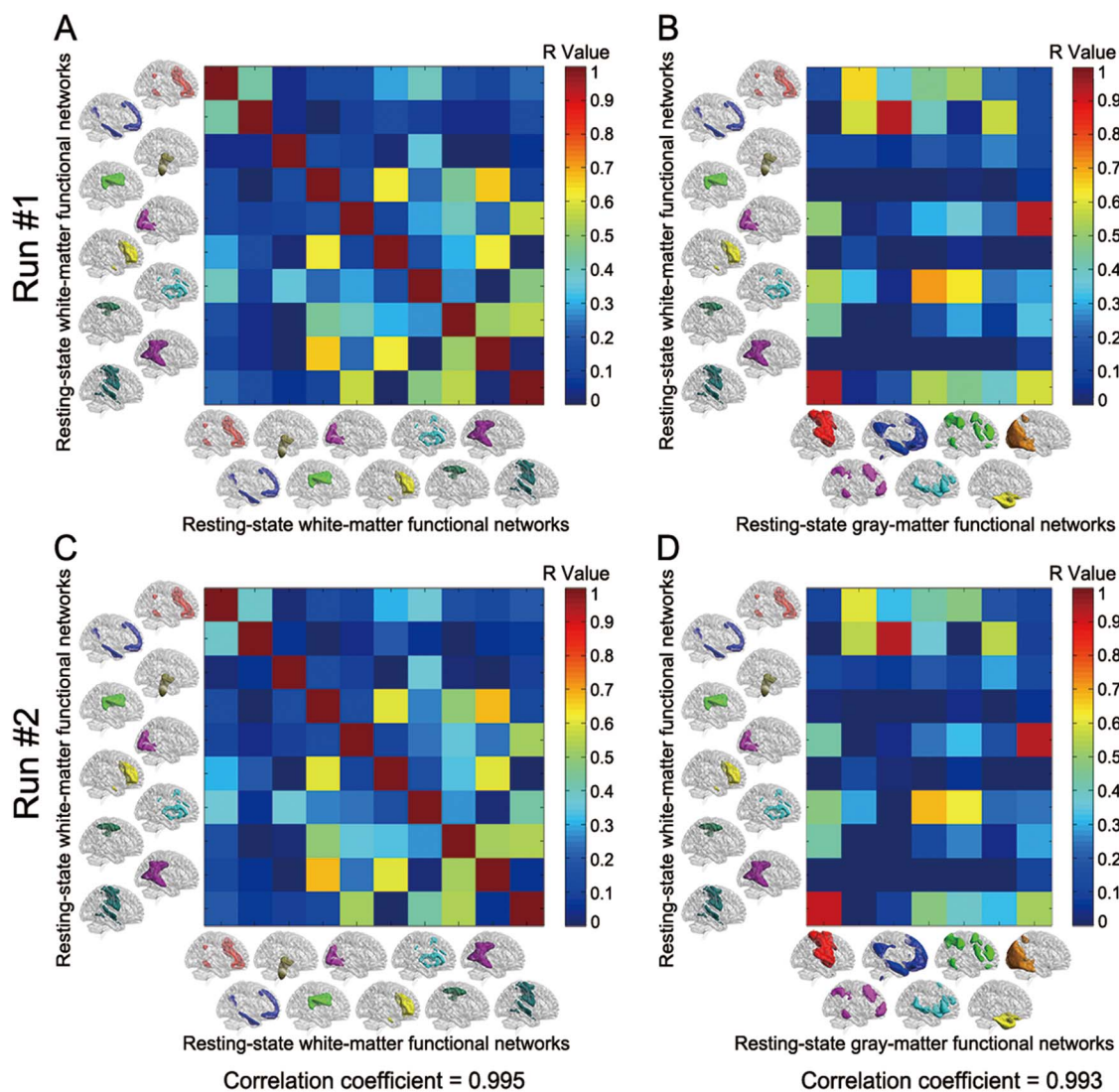
Figure 3. Functional connectivity of the WM-FNs in resting state. (A) and (C) show averaged functional connectivity strength between the different WM-FNs in run #1 and run #2 data, respectively. (B) and (D) show averaged functional connectivity strength between the WM-FNs and GM-FNs in run #1 and run #2 data, respectively. The colorbar shows the correlation coefficient. The reproducibility of functional connectivity of the WM-FNs is estimated by calculating the Pearson's correlation coefficient between averaged functional connectivity matrices from two runs.

WM-FNs were closely associated with the GM-FNs with the DMN, visual network, and sensorimotor network, respectively ($r > 0.9$, Fig. 3B). This association between WM- and GM-FNs might be attributed to the participation of WM-FNs in the support for brain functions together with GM-FNs (Jiang et al. 2019). Although the deep, orbitofrontal, and posterior corona radiata WM-FNs were not associated with any GM-FNs, they showed strong connection with other WM-FNs ($r > 0.5$, . 3A). For example, deep WM-FN (Fig. 2, 04) was not strongly associated with any GM-FNs ($r < 0.5$, Fig. 3B) but with orbitofrontal WM-FN (Fig. 2, 06) and posterior corona radiata WM-FN (Fig. 2, 09). These results suggest that certain WM-FNs indirectly participate in the whole brain functional integration.

The organization between the corpus callosum and WM-FNs was revealed in this study (Fig. 4). To the best of our knowledge, this is the first study that identified subregions of corpus callosum by using resting-state functional connectivity of white-matter BOLD signals. The corpus callosum is crucial for the functional integration between homotopic regions of the two hemispheres (Gazzaniga 2000). Studying subjects with different types of callosal lesions and callosotomies has significantly improved our understanding of the functional role of callosal subregions and brain function in general (Gazzaniga 2005). Moreover, the association between corpus callosum and other brain regions has been intensively studied, but most studies focused on cortical gray-matter regions and networks (de Lacoste et al. 1985; Huang et al. 2005; Hofer and Frahm 2006; Chao et al. 2009). As one of major white-matter fiber bundles, how the corpus callosum mediates functional information transfer remains unknown (van der Knaap and van der Ham 2011). In this study, we demonstrated that corpus callosum could be parcellated into 10 subregions, which functionally linked with superficial, middle, or deep WM-FNs (Fig. 4).
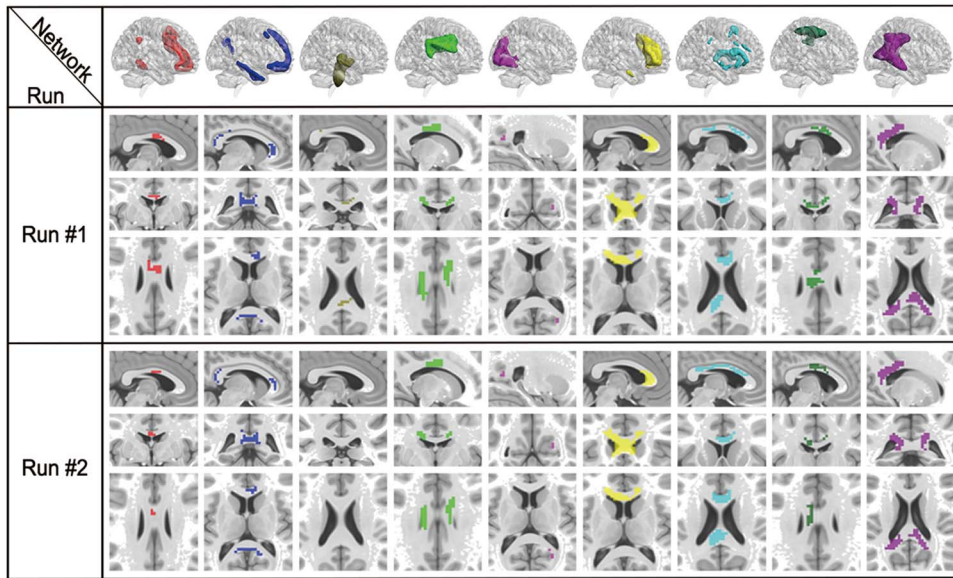
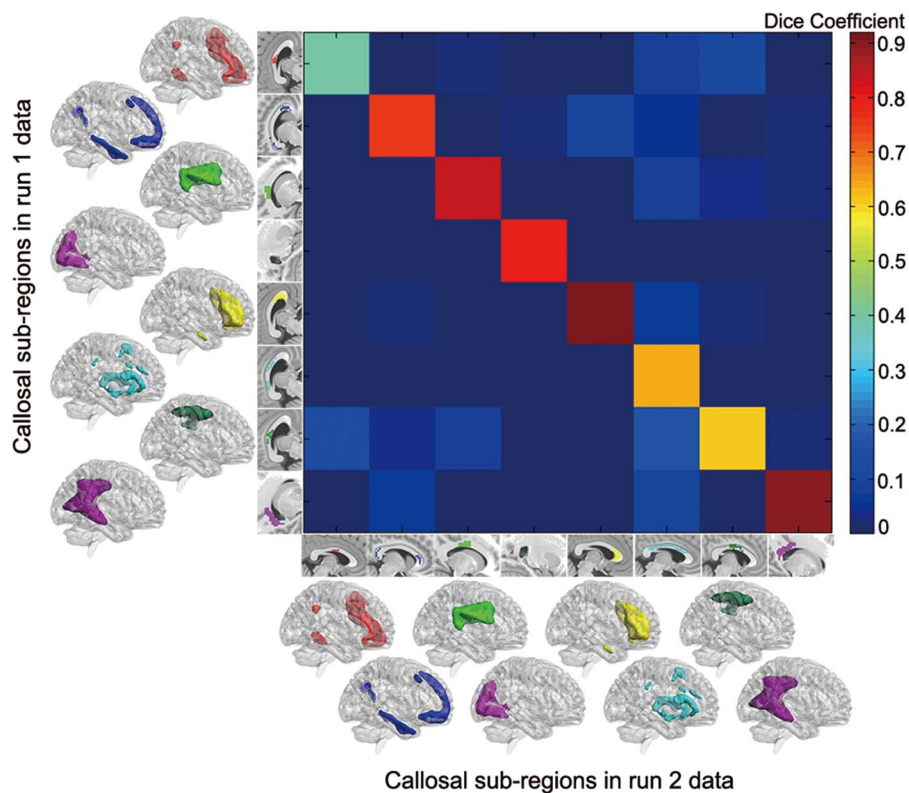**Figure 4.** Reproducible subregions of corpus callosum in the two runs using winner-take-all method.

Figure 5. The overlap between callosal subregions corresponding to each WM-FN from two runs. The x-axis represents the eight subregions of corpus callosum using run #1 data, and the y-axis represents the eight subregions of corpus callosum using run #2 data. The color bar shows the Dice coefficient between callosal subregions corresponding to each WM-FN from two runs.

For sensorimotor system, we found that the anterior mid-body, posterior midbody, and isthmus of corpus callosum were strongly connected with the deep and sensorimotor middle WM-FNs (Fig. 4). It is commonly acknowledged that these regions of corpus callosum are involved in the gray-matter sensorimotor

system (Witelson 1989; van der Knaap and van der Ham 2011). We also found sensorimotor superficial WM-FN was closely associated with sensorimotor middle WM-FN ($r > 0.5$, Fig. 3A) and gray-matter sensorimotor network ($r > 0.9$, Fig. 3B). However, the correlation between the sensorimotor superficial WM-FN

Table 1 The detailed specification of callosal subregion corresponding to each WM-FN in runs #1 and #2 data

Corresponding WM-FNs	Voxel size	Peak intensity (T)	MNI coordinate			Side
			x	y	z	
Left prefrontal WM-FN						
Run #1	20	6.47	6	−3	27	IH
Run #2	15	6.4	0	−3	27	IH
Tempofrontal WM-FN						
Run #1	61	24.22	12	30	−6	R
	51	16.71	9	−45	9	IH
Run #2	57	16.3	9	−45	9	IH
	44	19.89	12	30	−6	R
	4	8.11	0	−12	27	IH
Inferior corticospinal WM-FN						
Run #1	15	6.74	9	−27	30	IH
Run #2	—	—	—	—	—	—
Deep WM-FN						
Run #1	71	17.43	−18	−9	33	L
	54	23.17	15	3	30	R
Run #2	59	19.52	−18	−9	33	L
	53	18.64	15	−3	33	R
Occipital WM-FN						
Run #1	3	14.48	24	−60	12	R
Run #2	3	13.01	24	−60	12	R
Orbitofrontal WM-FN						
Run #1	320	36.95	18	24	21	IH
Run #2	314	29.85	−18	33	12	IH
Anterior corona radiata WM-FN						
Run #1	57	8.16	3	−15	27	IH
	40	14.48	6	21	18	IH
Run #2	199	13.25	6	21	18	IH
Sensorimotor middle WM-FN						
Run #1	50	9.79	−15	−15	36	L
	39	13.36	15	−18	36	R
Run #2	37	11.76	−15	−18	36	L
	14	11.12	15	−12	36	R
Posterior corona radiata WM-FN						
Run #1	321	37.02	−27	−51	18	IH
Run #2	303	29.95	−27	−51	21	IH
Sensorimotor superficial WM-FN						
Run #1	—	—	—	—	—	—
Run #2	—	—	—	—	—	—

IH (inter-hemisphere).

and corpus callosum was weak since we did not find any corresponding callosal voxels directly associated with sensorimotor superficial WM-FN. This might constitute the gradient information flow between corpus callosum, via intermediate white-matter and gray-matter sensorimotor cortex. Previous study on schizophrenia demonstrated that the dysfunctional association between gray-matter perception-motor system and the superficial WM-FNs was compensated through the middle-deep WM-FNs (Jiang et al. 2019). Such gradient functional organization might be beneficial for brain health.

The voxels of callosal subregion corresponding to the occipital WM-FN mainly concentrated on the splenium of corpus callosum. It is commonly acknowledged that the fiber bundles passing through the splenium of corpus callosum are related to the gray-matter occipital cortex connecting with visual system (Witelson 1989; van der Knaap and van der Ham 2011). We found that the occipital WM-FN has close relationship with gray-matter visual network ($r > 0.9$) (Fig. 3B,D).

The subregion of corpus callosum corresponding to the occipital WM-FN might participate in the adjustment of transmitting visual information between two hemispheres. Moreover, we found that the occipital WM-FN was closely associated with the sensorimotor superficial WM-FN ($r > 0.5$) (Fig. 3A). Several studies have revealed that the visual system has a close relationship with motor system (Held and Hein 1963; Goodale and Milner 1992; Loula et al. 2005). The visual systems process information either through the dorsal stream or the ventral stream. The parietal areas are key parts of dorsal stream, which is believed to process the visual information needed for understanding spatial relationships and controlling spatially directed actions (Mishkin et al. 1983; Nolte 2002; Milner and Goodale 2006). Our findings that the splenium of the corpus callosum was corresponded to the occipital WM-FN associated with sensorimotor superficial WM-FN may provide new clues to understand the mechanism of dorsal stream in cerebral visual system.
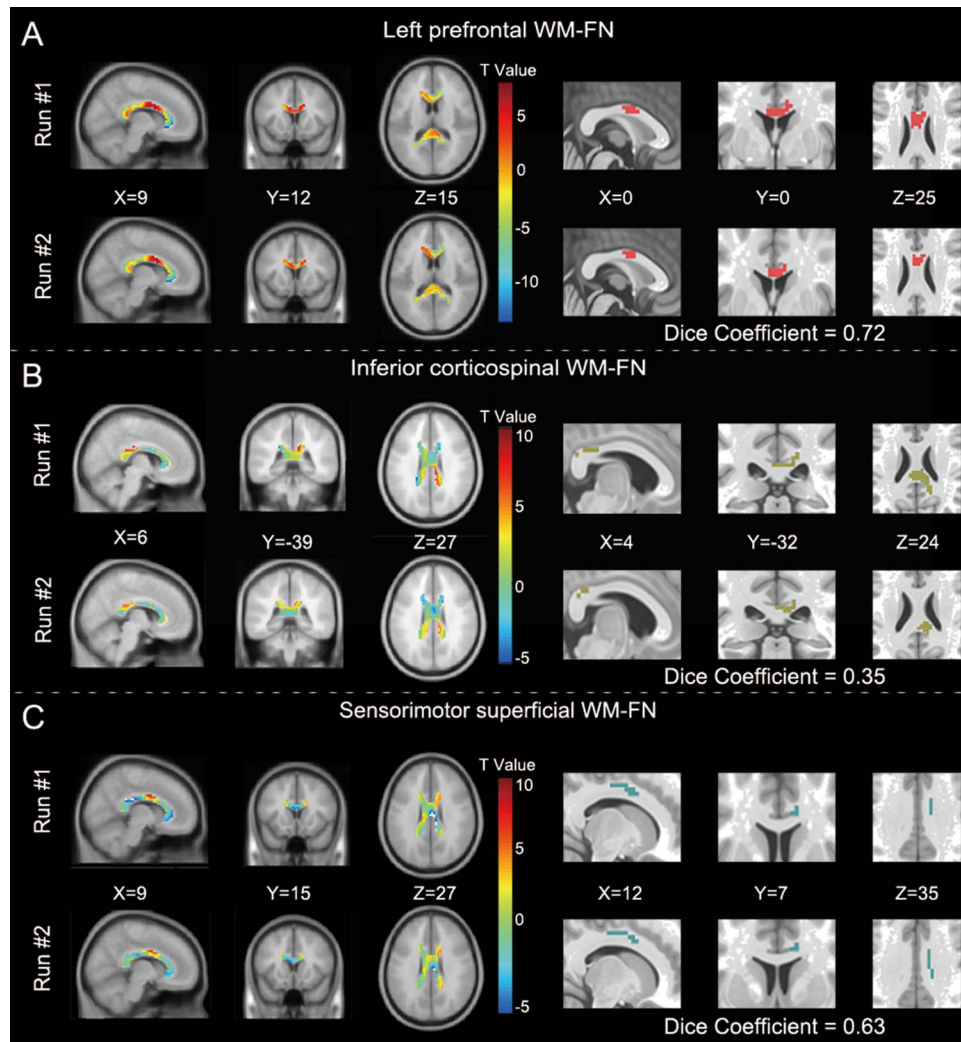
Figure 6. One-sample *t*-test maps and subregions of corpus callosum from the two different runs. The left side shows the results of callosal one-sample *t*-test maps. The right side shows the results of corrected maps to one-sample *t*-test maps (P < 0.05, FWE correction). The color bar shows the t value from the one-sample *t*-test. The Dice coefficient between callosal subregions corresponding to each WM-FN from two runs is shown.

We also found that callosal subregion in the splenium and genu of corpus callosum corresponded to the tempofrontal WM-FN (Fig. 4), which had a close relationship with the DMN (r > 0.9 Fig. 3B). The histological evidence suggests that these subregions of corpus callosum were structurally connected to the gray-matter occipital, inferior temporal, and prefrontal regions (Witelson 1989; van der Knaap and van der Ham 2011). This has been shown to be the main component distributed in the DMN. Callosal subregion corresponding to tempofrontal WM-FN was frequently associated with self-referential function (Greicius et al. 2003; Sheline et al. 2009).

For other higher order functional systems, four distributed subregions of corpus callosum were found in relation to left prefrontal, anterior/posterior corona radiata, and orbitofrontal WM-FNs (Fig. 4). First, anterior midbody of corpus callosum showed strong functional connectivity with left prefrontal WM-FN, which had a high correlation with the gray-matter fronto-parietal network (r = 0.64, Fig. 3B). This functional pathway might play a role in modulating cognitive control (Zanto and Gazzaley 2013). Second, as for the subregion of corpus callosum

corresponding to the anterior corona radiata WM-FN, it was found to be distributed in seven areas of corpus callosum having been previously reported (Witelson 1989; van der Knaap and van der Ham 2011). Furthermore, anterior corona radiata WM-FN was associated with the gray-matter ventral attention network, which suggested this callosal subregion might be associated with detecting unattended or unexpected stimuli and triggering shifts of attention. (Shulman et al. 2002). Third, the subregion of corpus callosum corresponding to the posterior corona radiata WM-FN was located in the isthmus and splenium of corpus callosum defined by Witelson and colleagues (Witelson 1989). Fourth, the subregion of corpus callosum corresponding to the orbitofrontal WM-FN, mainly included the rostral and genu of corpus callosum. Notably, the posterior corona radiata and orbitofrontal WM-FNs were not strongly connected with any GM-FNs (r < 0.5, Fig. 3B), but they were connected with other WM-FNs and corpus callosum (Figs 3 and 4), which enabled them to be involved in maintaining normal brain function.

In this study, we tested the reproducibility of our findings in the second resting-state run. We found that the

associations between identified callosal subregions and WM-FNs were consistent in two runs, which suggested a high reproducibility (Fig. 5). Additionally, the inferior corticospinal and sensorimotor superficial WM-FNs had no corresponding voxel in the corpus callosum across participants in run1 and/or run2. This might be due to the winner-take-all method, which assumes only a single network exists (Buckner et al. 2011). Therefore, we used different strategy (one-sample *t*-test with FWE correction) for the left prefrontal, inferior corticospinal, and sensorimotor superficial WM-FNs, according to prior study (Yuan et al. 2016). We found that the Dice coefficients for callosal subregions corresponding to the left prefrontal and sensorimotor superficial WM-FNs were within the moderate–high level (Fig. 6). These results suggest that the callosal subregions corresponding to the left prefrontal and sensorimotor superficial WM-FNs are reproducible (the one-sample *t*-test maps and FWE-corrected results for the other seven WM-FNs were displayed in Fig. S3–1). In sum, the associations between WM-FNs and corpus callosum were reproducible.

The present study described a new approach of dividing the corpus callosum into different subregions using resting-state functional connectivity. To more fully understand the connection between the corpus callosum and the brain's functional organization, we reviewed previous studies parcellating the corpus callosum using different approaches such as those described within microscopy and DTI approaches (Table S6–1) (Aboitiz et al. 1992; Huang et al. 2005; Hofer and Frahm 2006; Zarei et al. 2006; Chao et al. 2009; Archer et al. 2019). We compared our corpus callosum parcellation results with previous results using other methods and found that they had a high similarity. Specifically, first the sensorimotor superficial WM-FN, related with gray-matter sensorimotor networks ($r > 0.9$) (Fig. 3), was closely linked with the anterior midbody of corpus callosum (Fig. 4). The sensorimotor middle WM-FN was associated with the anterior midbody, isthmus, and posterior midbody of corpus callosum. Previous callosal segmentation studies revealed that the isthmus, anterior midbody, and posterior midbody of corpus callosum were correlated to the gray-matter motor and somatosensory cortical areas, which was consistent with our callosal subregions corresponding to the sensorimotor superficial and sensorimotor middle WM-FNs (Hofer and Frahm 2006; Chao et al. 2009; Archer et al. 2019). Second, the occipital WM-FN that was closely related with the gray-matter visual network ($r > 0.9$) (Fig. 3) was associated with the splenium of the corpus callosum (Fig. 4), which was consistent with previous callosal subregions corresponding to the occipital lobe (Table S6–1). Third, the tempofrontal WM-FN, associated with the DMN ($r > 0.9$) (Fig. 3), was closely related with the splenium and the genu of the corpus callosum that was confirmed to correspond to the temporal and frontal lobes (Table S6–1). Here, we mainly compared some subregions of corpus callosum that corresponded to WM-FNs closely related with GM-FNs ($r > 0.9$). For the remaining segmentation results of the corpus callosum, see Table S6–1. A comparison with previous callosal segmentation results suggested that our callosal parcellation results were reliable and consistent with previous results.

Limitations

This study has several limitations. First, some researchers have speculated that the BOLD signal from white matter may have infiltrated from the gray-matter due to partial volume effect. To minimize the partial volume effect and the influence of gray-matter signals, we performed the spatial smoothing on white-matter and gray-matter separately and used only voxels identified as white matter for each subject. Second, this study did not have the structural connection results for the WM-FNs or corpus callosum. However, other studies have demonstrated DTI-based connections of WM-FNs (Peer et al. 2017) and corpus callosum (Huang et al. 2005; Chao et al. 2009) separately. Future research is needed to characterize the relationship between the WM-FNs and corpus callosum combining with diffusion tensor imaging (DTI) data. Third, to measure the reproducibility of our results, we used two runs of data to analyze WM-FNs and subregions of corpus callosum. Although the results of the two sets of data were highly consistent, there were some differences with the inferior corticospinal WM-FN. Though it may be due to the lower BOLD signal quality in the brainstem area, future research is needed to further evaluate these WM-FNs. Finally, it is unclear whether the fMRI parameters optimized for the GM are also reliable for these studies investigating the white-matter BOLD signal. Future research is needed to analyze the white-matter BOLD signal.

Conclusion

The current study demonstrates that the corpus callosum connecting different WM-FNs has functional segmentation and spatial distribution patterns. In addition, different callosal subregions might be responsible for various cognitive functions of the brain. Several previous studies and our study have revealed the close relationship between WM- and GM-FNs. Our study has provided more detailed pathway patterns of brain function between the corpus callosum and brain functional networks, which might be important for better understanding the whole brain organization of primary and higher order functional systems.

Funding

References

Aboitiz F, Scheibel AB, Fisher RS, Zaidel E. 1992. Fiber composition of the human corpus-callosum. *Brain Res*. 598:143–153.

Arai K, Lo EH. 2009. Oligovascular Signaling in white matter stroke. *Biol Pharm Bull*. 32:1639–1644.

Archer DB, Coombes SA, McFarland NR, DeKosky ST, Vaillancourt DE. 2019. Development of a transcallosal tractography template and its application to dementia. *NeuroImage*. 200:302–312.

Babalola KO, Patenaude B, Aljabar P, Schnabel J, Kennedy D, Crum W, Smith S, Cootes T, Jenkinson M, Rueckert D. 2010. An evaluation of four automatic methods of segmenting the subcortical structures in the brain vol 47, pg 1435, 2009. *NeuroImage*. 49:1152–1152.

Baumgardner TL, Singer HS, Denckla MB, Rubin MA, Abrams MT, Colli MJ, Reiss AL. 1996. Corpus callosum morphology in children with Tourette syndrome and attention deficit hyperactivity disorder. *Neurology*. 47:477–482.

Berlucchi G. 1983. Two hemispheres but one brain. *Behav Brain Sci.* 6:171–172.

Biswal B, Yetkin FZ, Haughton VM, Hyde JS. 1995. Functional connectivity in the motor cortex of resting human brain using echo-planar mri. *Magn Reson Med.* 34:537–541.

Blumensath T, Jbabdi S, Glasser MF, Van Essen DC, Ugurbil K, Behrens TEJ, Smith SM. 2013. Spatially constrained hierarchical parcellation of the brain with resting-state fMRI. *NeuroImage.* 76:313–324.

Buckner RL, Krienen FM, Castellanos A, Diaz JC, Yeo BTT. 2011. The organization of the human cerebellum estimated by intrinsic functional connectivity. *J Neurophysiol.* 106:2322–2345.

Chao Y-P, Cho K-H, Yeh C-H, Chou K-H, Chen J-H, Lin C-P. 2009. Probabilistic topography of human corpus callosum using cytoarchitectural parcellation and high angular resolution diffusion imaging tractography. *Hum Brain Mapp.* 30:3172–3187.

Courtemanche MJ, Sparrey CJ, Song X, MacKay A, D'Arcy RCN. 2018. Detecting white matter activity using conventional 3 tesla fMRI: an evaluation of standard field strength and hemodynamic response function. *NeuroImage.* 169:145–150.

Craddock RC, James GA, Holtzheimer PE III, Hu XP, Mayberg HS. 2012. A whole brain fMRI atlas generated via spatially constrained spectral clustering. *Hum Brain Mapp.* 33:1914–1928.

de Lacoste MC, Kirkpatrick JB, Ross ED. 1985. Topography of the human corpus callosum. *J Neuropathol Exp Neurol.* 44:578–591.

Desikan RS, Segonne F, Fischl B, Quinn BT, Dickerson BC, Blacker D, Buckner RL, Dale AM, Maguire RP, Hyman BT, et al. 2006. An automated labeling system for subdividing the human cerebral cortex on MRI scans into gyral based regions of interest. *NeuroImage.* 31:968–980.

Ding Z, Huang Y, Bailey SK, Gao Y, Cutting LE, Rogers BP, Newton AT, Gore JC. 2018. Detection of synchronous brain activity in white matter tracts at rest and under functional loading. *Proc Natl Acad Sci U S A.* 115:595–600.

Fabri M, Polonara G, Mascioli G, Salvolini U, Manzoni T. 2011. Topographical organization of human corpus callosum: an fMRI mapping study. *Brain Res.* 1370:99–111.

Gawryluk JR, Mazerolle EL, D'Arcy RCN. 2014. Does functional MRI detect activation in white matter? A review of emerging evidence, issues, and future directions. *Front Neurosci.* 8:239.

Gazzaniga MS. 2000. Cerebral specialization and interhemispheric communication-does the corpus callosum enable the human condition? *Brain.* 123:1293–1326.

Gazzaniga MS. 2005. Forty-five years of split-brain research and still going strong. *Nat Rev Neurosci.* 6:653–U651.

Giedd JN, Blumenthal J, Jeffries NO, Rajapakse JC, Vaituzis AC, Liu H, Berry YC, Tobin M, Nelson J, Castellanos FX. 1999. Development of the human corpus callosum during childhood and adolescence: a longitudinal MRI study. *Prog Neuro-Psychopharmacol Biol Psychiatry.* 23:571–588.

Giedd JN, Castellanos FX, Casey BJ, Kozuch P, King AC, Hamburger SD, Rapoport JL. 1994. Quantitative morphology of the corpus-callosum in attention-deficit hyperactivity disorder. *Am J Psychiatr.* 151:665–669.

Goodale MA, Milner AD. 1992. Separate visual pathways for perception and action. *Trends Neurosci.* 15:20–25.

Greicius MD, Krasnow B, Reiss AL, Menon V. 2003. Functional connectivity in the resting brain: a network analysis of the default mode hypothesis. *Proc Natl Acad Sci U S A.* 100:253–258.

Harris JJ, Attwell D. 2012. The energetics of CNS white matter. *J Neurosci.* 32:356–371.

Held R, Hein A. 1963. Movement-produced stimulation in the development of visually guided behavior. *J Comp Physiol Psychol.* 56:872–876.

Hofer S, Frahm J. 2006. Topography of the human corpus callosum revisited-comprehensive fiber tractography using diffusion tensor magnetic resonance imaging. *NeuroImage.* 32:989–994.

Huang H, Zhang JY, Jiang HY, Wakana S, Poetscher L, Miller MI, van Zijl PCM, Hillis AE, Wytik R, Mori S. 2005. DTI tractography based parcellation of white matter: application to the mid-sagittal morphology of corpus callosum. *NeuroImage.* 26:195–205.

Huang Y, Bailey SK, Wang P, Cutting LE, Gore JC, Ding Z. 2018. Voxel-wise detection of functional networks in white matter. *NeuroImage.* 183:544–552.

Ji G-J, Liao W, Chen F-F, Zhang L, Wang K. 2017. Low-frequency blood oxygen level-dependent fluctuations in the brain white matter: more than just noise. *Sci Bull.* 62:656–657.

Jiang Y, Luo C, Li X, Li Y, Yang H, Li J, Chang X, Li H, Yang H, Wang J, et al. 2019. White-matter functional networks changes in patients with schizophrenia. *NeuroImage.* 190:172–181.

Lorio S, Fresard S, Adaszewski S, Kherif F, Chowdhury R, Frackowiak RS, Ashburner J, Helms G, Weiskopf N, Lutti A, et al. 2016. New tissue priors for improved automated classification of subcortical brain structures on MRI. *NeuroImage.* 130:157–166.

Loula F, Prasad S, Harber K, Shiffrar M. 2005. Recognizing people from their movement. *J Exp Psychol Hum Percept Perform.* 31:210–220.

Lowe MJ, Mock BJ, Sorenson JA. 1998. Functional connectivity in single and multislice echoplanar imaging using resting-state fluctuations. *NeuroImage.* 7:119–132.

Marussich L, Lu K-H, Wen H, Liu Z. 2017. Mapping white-matter functional organization at rest and during naturalistic visual perception. *NeuroImage.* 146:1128–1141.

Mazerolle EL, D'Arcy RCN, Beyea SD. 2008. Detecting functional magnetic resonance imaging activation in white matter: interhemispheric transfer across the corpus callosum. *BMC Neurosci.* 9.

Milner D, Goodale M. 2006. *The Visual Brain in Action.* New York: Oxford University Press.

Mishkin M, Ungerleider LG, Macko KA. 1983. Object vision and spatial vision: two cortical pathways. *Trends Neurosci.* 6:414–417.

Mori S, Oishi K, Jiang H, Jiang L, Li X, Akhter K, Hua K, Faria AV, Mahmood A, Woods R, et al. 2008. Stereotaxic white matter atlas based on diffusion tensor imaging in an ICBM template. *NeuroImage.* 40:570–582.

Nolte J. 2002. The human brain: an introduction to its functional neuroanatomy. *Mosby: St Louis.*

Ogawa S, Lee TM, Kay AR, Tank DW. 1990. Brain magnetic resonance imaging with contrast dependent on blood oxygenation. *Proc Natl Acad Sci U S A.* 87:9868–9872.

Peer M, Nitzan M, Bick AS, Levin N, Arzyt S. 2017. Evidence for functional networks within the human brain's white matter. *J Neurosci.* 37:6394–6407.

Power JD, Barnes KA, Snyder AZ, Schlaggar BL, Petersen SE. 2012. Spurious but systematic correlations in functional connectivity MRI networks arise from subject motion (vol 59, pg 2142, 2012). *NeuroImage.* 63:999–999.

Rosas HD, Lee SY, Bender AC, Zaleta AK, Vangel M, Yu P, Fischl B, Pappu V, Onorato C, Cha JH, *et al*. 2010. Altered white matter microstructure in the corpus callosum in Huntington's disease: implications for cortical "disconnection". *NeuroImage*. 49:2995–3004.

Satterthwaite TD, Elliott MA, Gerraty RT, Ruparel K, Loughead J, Calkins ME, Eickhoff SB, Hakonarson H, Gur RC, Gur RE, *et al*. 2013. An improved framework for confound regression and filtering for control of motion artifact in the preprocessing of resting-state functional connectivity data. *NeuroImage*. 64:240–256.

Sebire G, Goutieres F, Tardieu M, Landrieu P, Aicardi J. 1995. Extensive macrogyri or no visible gyri - distinct clinical, electroencephalographic, and genetic features according to different imaging patterns. *Neurology*. 45:1105–1111.

Sheline YI, Barch DM, Price JL, Rundle MM, Vaishnavi SN, Snyder AZ, Mintun MA, Wang S, Coalson RS, Raichle ME. 2009. The default mode network and self-referential processes in depression. *Proc Natl Acad Sci U S A*. 106:1942–1947.

Shulman GL, d'Avossa G, Tansy AP, Corbetta M. 2002. Two attentional processes in the parietal lobe. *Cereb Cortex*. 12:1124–1131.

Teo PC, Sapiro G, Wandell BA. 1997. Creating connected representations of cortical gray matter for functional MRI visualization. *IEEE Trans Med Imaging*. 16:852–863.

van der Knaap LJ, van der Ham IJM. 2011. How does the corpus callosum mediate interhemispheric transfer? A review. *Behav Brain Res*. 223:211–221.

Van Essen DC, Smith SM, Barch DM, Behrens TEJ, Yacoub E, Ugurbil K, WU-MH C. 2013. The WU-Minn human connectome project: an overview. *NeuroImage*. 80:62–79.

Vermersch P, Roche J, Hamon M, DaemsMonpeurt C, Pruvo JP, Dewailly P, Petit H. 1996. White matter magnetic resonance imaging hyperintensity in Alzheimer's disease: correlations with corpus callosum atrophy. *J Neurol*. 243:231–234.

Wilson SM, Bautista A, Yen M, Lauderdale S, Eriksson DK. 2017. Validity and reliability of four language mapping paradigms. *Neuroimage Clin*. 16:399–408.

Witelson SF. 1989. Hand and sex differences in the isthmus and genu of the human corpus callosum. A postmortem morphological study. *Brain J Neurol*. 112(Pt 3): 799–835.

Woodruff PWR, McManus IC, David AS. 1995. Metaanalysis of corpus-callosum size in schizophrenia. *J Neurol Neurosurg Psychiatry*. 58:457–461.

Wu X, Yang Z, Bailey SK, Zhou J, Cutting LE, Gore JC, Ding Z. 2017. Functional connectivity and activity of white matter in somatosensory pathways under tactile stimulations. *NeuroImage*. 152:371–380.

Yarkoni T, Barch DM, Gray JR, Conturo TE, Braver TS. 2009. BOLD correlates of trial-by-trial reaction time variability in gray and white matter: a multi-study fMRI analysis. *PLoS One*. 4:e4257.

Yazgan MY, Wexler BE, Kinsbourne M, Peterson B, Leckman JF. 1995. Functional-significance of individual variations in callosal area. *Neuropsychologia*. 33:769–779.

Yeo BTT, Krienen FM, Chee MWL, Buckner RL. 2014. Estimates of segregation and overlap of functional connectivity networks in the human cerebral cortex. *NeuroImage*. 88: 212–227.

Yeo BTT, Krienen FM, Sepulcre J, Sabuncu MR, Lashkari D, Hollinshead M, Roffman JL, Smoller JW, Zoeller L, Polimeni JR, *et al*. 2011. The organization of the human cerebral cortex estimated by intrinsic functional connectivity. *J Neurophysiol*. 106:1125–1165.

Yuan R, Di X, Taylor PA, Gohel S, Tsai Y-H, Biswal BB. 2016. Functional topography of the thalamocortical system in human. *Brain Struct Funct*. 221:1971–1984.

Zanto TP, Gazzaley A. 2013. Fronto-parietal network: flexible hub of cognitive control. *Trends Cogn Sci*. 17:602–603.

Zarei M, Johansen-Berg H, Smith S, Ciccarelli O, Thompson AJ, Matthews PM. 2006. Functional anatomy of interhemispheric cortical connections in the human brain. *J Anat*. 209: 311–320.

Zhang K, Sejnowski TJ. 2000. A universal scaling law between gray matter and white matter of cerebral cortex. *Proc Natl Acad Sci U S A*. 97:5621–5626.